Advances in Sustainable Energies & Environment

Journal homepage: https://A-SEE.MazUST.ac.ir/

Research Article

CuBTC Metal–Organic Framework Modified with Functionalized Activated Carbon for Improved CO_2/H_2 Selectivity

Kourosh Esfandiari

Department of Chemical Engineering, Babol Noshirvani University of Technology, Babol, Mazandaran, Iran

ARTICLE INFO

Article history:
Received: 2025-07-20
Revised: 2025-11-02
Accepted: 2025-12-03
Published online: 2026-01-01

Keywords:
MOF;
Activated carbon;
CuBTC;
Composite material;
Gas separation.

ABSTRACT

This study explores the solvothermal synthesis and gas separation performance of composite materials composed of CuBTC, a prototypical metal–organic framework, and functionalized activated carbon (AC). The materials were prepared with varying amounts of AC to assess their effectiveness in selective CO_2/H_2 separation. Selectivity measurements were conducted using a volumetric–chromatographic approach. Structural and morphological properties of the composites were characterized by powder X-ray diffraction (XRD), nitrogen adsorption–desorption analysis, and field emission scanning electron microscopy (FESEM). The XRD data confirmed that the crystalline integrity of CuBTC remained unchanged in the presence of AC, indicating compatibility between the two components. Notably, the composite containing 0.050 g of functionalized AC exhibited a CO_2/H_2 separation factor of approximately 32, which is more than twice that of pristine CuBTC (~15) under ambient conditions (298 K, low pressure). The enhanced separation performance is attributed to carbonyl and nitro groups on the AC surface, which promote preferential CO_2 adsorption within the CuBTC–AC composite structure.

GRAPHICAL ABSTRACT

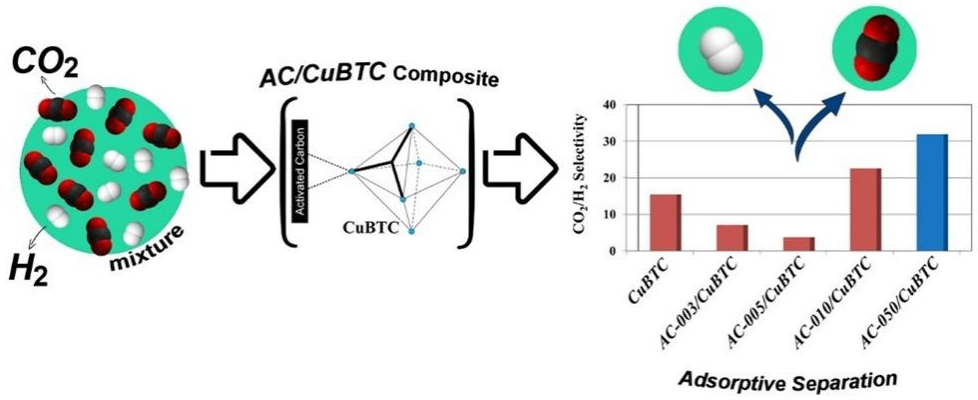

*** Corresponding author.**
E-mail address: *kourosh.esfandiari@gmail.com*

Cite this article as:

Esfandiari, K. (2026). CuBTC Metal–Organic Framework Modified with Functionalized Activated Carbon for Improved CO_2/H_2 Selectivity. *Advances in Sustainable Energies & Environment.* https://doi.org/10.22034/a-see.2025.2066417.1003

1. Introduction

Hydrogen energy is widely recognized as a clean and carbon-free energy source, characterized by minimal pollutant emissions during combustion. Currently, approximately 95% of global hydrogen production is derived from steam methane reforming (SMR), which remains the most commercially prevalent method [1]. The effluent gas from SMR primarily consists of hydrogen (H_2), accompanied by trace impurities including carbon dioxide (CO_2), carbon monoxide (CO), nitrogen (N_2), and water vapor (H_2O). In order to utilize these hydrogen-rich streams as a clean energy source, further purification processes are essential. Among the existing contaminants, CO_2 is the most abundant [2, 3], thus rendering its selective removal pivotal for effective hydrogen enrichment.

Metal-organic frameworks (MOFs) constitute a well-established class of porous materials, distinguished by their exceptional adsorption and separation capabilities. Their tunable structures, high specific surface area (SSA), and substantial pore volumes render them promising candidates for a wide range of applications [4]. However, studies have indicated that the extensive void space inherent in MOF matrices does not entirely contribute to adsorption and separation processes [5].

One promising strategy to compensate for the weak interactions between guest molecules and internal pores involves the fabrication of composite materials by assembling secondary porous structures—particularly carbon-based materials—with metal–organic frameworks (MOFs). Among these, carbon nanotubes (CNTs) [6-11], graphene oxides (GOs) [12-15], and activated carbons (ACs) have been widely employed as functional components in MOF-based composites. Concerning AC/MOF composites where AC is incorporated into the MOF matrix, Bajaj et al. [16], incorporated AC particles within the CuBTC matrix with the purpose of higher methane adsorption. Somayajulu Rallapalli et al. [17] assessed the potential of incorporating microporous AC in MIL-101 to achieve higher H_2 uptakes. Lee and Park [18] enhanced the H_2 storage capacity of a well-known Zn-based MOF, i.e., MOF-5, by doping platinum on AC particles and incorporating AC into the MOF matrix. Prabhakaran and Deschamps [19] demonstrated the higher hydrogen adsorption of MIL-101 modified by AC and lithium doping. Mahmoodi et al. [20] removed Acid Green 25 (AG25) and Reactive Yellow 186 (RY186) dyes from colored wastewaters using AC incorporated MIL-101(Cr) and demonstrated that higher amounts of AC can enhance dye removal ability of the synthesized composite. McHugh et al. [21] prepared a composite material where STAM-17-OEt MOF was incorporated into the commercially available BPL activated carbon (i.e., STAM-17-OEt@BPL) and showed enhanced adsorptive characteristics of the composite in comparison to both the primary MOF and carbon materials. In a prior work, we demonstrated that the hydrogen storage capacity of CuBTC can be improved by introducing an optimal amount of activated carbon (AC) during the composite synthesis process [22].

Although AC can be utilized as a promising candidate to make a composite material with MOFs, However, bare activated carbon is relatively non-polar and its interaction with CO_2 (a quadrupolar molecule) is limited. Hence, introducing chemical groups onto the carbon surface, can enhance both adsorption capacity and selectivity for CO_2 over other gases. From the perspective of functionalization, extensive studies have been reported so far introducing different functional groups on AC such as nitrogen- or oxygen-containing groups (amine, nitro, carboxyl, hydroxyl, carbonyl, etc.) for enhanced adsorption and separation of CO_2 [23-26]. With respect to AC/MOF composites, while carboxyl groups play the role of nucleation sites for composite formation, carbonyl and nitro groups have the merit of high CO_2 affinity, desirable for enhanced CO_2/H_2 separation purposes [27].

In this research, a CuBTC-based structure with enhanced textural properties was considered, and composite materials were synthesized by combining varying amounts of functionalized activated carbon (AC) with CuBTC through a solvothermal approach. Subsequently, the CO_2 sequestration performance of the resulting AC/CuBTC composites was assessed using volumetric–chromatographic measurements on a 50:50 (v/v) binary CO_2/H_2 gas mixture.

2. Materials and Methods

2.1. Chemicals

Copper (II) nitrate trihydrate ($Cu(NO_3)_2.3H_2O$), benzene-1,3,5-tricarboxylic acid (trimesic acid or H_3BTC), Sodium hydroxide (NaOH), nitric acid (HNO_3, 65 %wt), ortho-Phosphoric acid (H_3PO_4, 85 %wt), and pure ethanol were purchased from Merck (Germany) and were used as received without further purification. The purity of H_2 and CO_2 was 99.999% and 99.95%, respectively. Furthermore, a ~50:50 (v/v) mixture of H_2/CO_2 was purchased from Faran Sanat Mehr Co., Tehran, Iran.

2.2. Synthesis of Bare CuBTC

The synthesis of CuBTC was carried out by dissolving 1.75 g of copper (II) nitrate trihydrate (as the metal precursor) and 1.0 g of benzene-1,3,5-tricarboxylic acid (H_3BTC, as the organic linker) in 60 mL of absolute ethanol under ambient conditions. The resulting solution was stirred for 30 minutes and subsequently transferred into a 100 mL Teflon-lined stainless-steel autoclave. The autoclave was securely sealed and heated at 130 °C for 16 hours. Upon completion of the thermal treatment, the system was allowed to cool to room temperature. The formed CuBTC crystals were recovered via centrifugation (9000 rpm, 10 min, repeated three times), washed with ethanol after each cycle, and finally dried overnight at 100 °C.

2.3. Synthesis and Functionalization of AC

Synthesis and functionalization of AC was performed according to our previous research [22].

Walnut shells from Mazandaran (Northern Iran) were used as the precursor for activated carbon (AC). After crushing and sieving (<2 mm), the shells were soaked in 0.2 M NaOH for 20 h to remove residues and impurities, then rinsed with hot water to neutral pH and dried at 100°C overnight. Carbonization was performed at 350°C for 30 min under nitrogen atmosphere. The resulting char was impregnated with H_3PO_4 (4:1 weight ratio) and pyrolyzed at 500°C for 1 h in nitrogen. The product was washed with hot deionized water and dried at 110°C for 24 h. In addition, for achieving an AC with superior textural properties containing carboxyl functional groups on its surface), we washed as-synthesized AC with HNO_3 solution in a posterior treating step.

2.4. Synthesis of AC/CuBTC Composite

The synthesis procedure for AC/CuBTC composites closely follows that of pristine CuBTC. In this approach, a predetermined amount of acid-treated activated carbon (AC) was introduced into the initial MOF precursor solution comprising the metal salt, organic linker, and solvent. The mixture was stirred for 15 minutes and subsequently subjected to ultrasonic treatment (15 minutes; 100 kW; 400 Hz) before being transferred to a Teflon-lined stainless-steel autoclave for solvothermal reaction. The subsequent steps were carried out identically to the pure CuBTC synthesis protocol. Table 1 outlines the various AC loadings employed for composite formation. It is noteworthy that AC additions exceeding 0.050 g resulted in the emergence of a dispersed black solid phase in the final product, presumed to be unreacted AC. Accordingly, the upper limit for AC content in the synthesis solution was set at 0.050 g to ensure phase homogeneity and reproducibility.

2.5. Characterization Techniques

The powder X-ray diffraction (PXRD) patterns were collected on a PANalytical X'Pert Pro diffractometer (The Netherlands) in the range of 5º to 45º (2θ). In addition, the Scherrer equation was employed to determine the crystal size of as-synthesized samples based on XRD data according to the following equation [28]:

$$\tau = \frac{K.\lambda}{\beta.\cos\theta} \quad (1)$$

Where τ is the crystal size (nm), K is a dimensionless shape factor which is typically considered equal to 0.89, λ is the X-ray wavelength (0.154 nm in the case of CuKa1), β is the full width at half maximum intensity of the peak (FWHM) in radians, and θ is the Bragg angle of the diffraction peak in radians. The Brunauer–Emmett–Teller (BET) surface area of as-synthesized samples was determined by Belsorp Mini II (Japan). The morphology and structure of samples were studied with field emission scanning electron microscope (FESEM) images using Tescan MIRA3 FEG (Czech Republic) with an acceleration voltage of 5.0 kV. Finally, the composition of gas mixtures was analyzed by an Agilent 7890A gas chromatograph (USA) using helium as the sweeping gas. In addition, to determine the CO_2/H_2 separation factor of samples, a volumetric-chromatographic technique was used, which is described in the following section in detail.

2.6. Volumetric-Chromatographic Measurements

Single gas adsorption measurements were carried out in an apparatus comprising two similar vessels, so-called "*Load Cell*" and "*Adsorption Cell*" (Figure 1), which are connected with a valve (i.e., adsorption valve, Figure 1). The apparatus is equipped with a sensitive pressure sensor (Leo 2, Keller, Switzerland) to measure the pressure inside the load cell and the whole volume of the apparatus. In addition, to keep the temperature constant during the adsorption process, the cells are placed in a water bath (Memmert WaterBath WNB, Germany) capable of controlling the bath temperature using an electrical heating system. The adsorption pressure was increased gradually to draw the adsorption isotherm for each sample, which was previously placed in the "Adsorption Cell". It is worth noting that, the samples were activated by heating at 150°C overnight before each adsorption experiment.

Table 1. Summary of *AC/CuBTC* composites and the amount of AC in their structure

Amount of *AC* (g)	AC/CuBTC Composite
0.003	*AC-003/CuBTC*
0.005	*AC-005/CuBTC*
0.010	*AC-010/CuBTC*
0.050	*AC-050/CuBTC*

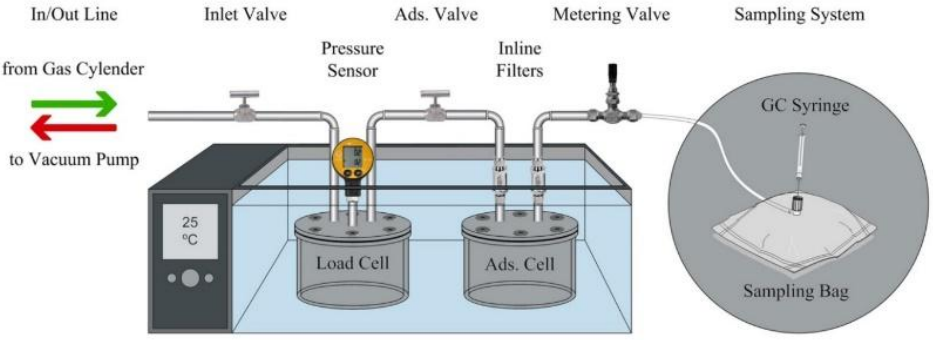

Fig. 1. Schematic diagram of volumetric adsorption apparatus equipped with a sampling line

For binary gas experiments, the aforementioned apparatus was equipped with a precise needle valve (known as a metering valve) to take a low-pressure sample from the gaseous mixture maintained above the adsorbent surface after the equilibrium was reached (Figure 1). The obtained sample was then injected into the gas chromatograph to determine the CO_2/H_2 composition.

Since the composition of the obtained samples from the adsorption cell (which is determined by gas chromatography) is not identical with the composition of the adsorbed phase within the adsorbent, an analytical approach was employed to determine the amounts of competitive adsorption of each CO_2 and H_2 on the adsorbent [28]. For this purpose, assume that a known amount of gas mixture available in the "*Load Cell*", is expanded into the "*Adsorption Cell*" and partially adsorbed on a certain mass of adsorbent, m^s. The overall mass balance during this adsorption process can be written as Eq. (2), where m^* (kg) is the mass of initial gas stored in the *Load Cell*, m^f (kg) is the mass of gas remained on the surface of the solid (not adsorbed), and m (kg) is the mass adsorbed on the porous solid after the equilibrium reached. This material balance is also true for each component *i* as well (Eq. 3). The purpose of this procedure is to determine the mass of component *i* adsorbed on the porous solid (m_i).

$$m^* = m^f + m \tag{2}$$

$$m_i^* = m_i^f + m_i \tag{3}$$

The total mass remaining on the surface of the solid (m^f) can be found as below:

$$m^f = \rho^f (V^* - V^V) \tag{4}$$

Where ρ^f is the density of gas at the bulk phase (kg/m^3) on the surface of the solid, V^* is the total volume (m^3) of the experimental apparatus (Figure 1), and V^V is the void volume (m^3), which indicates the inaccessible volume to adsorbing molecules in the *Adsorption Cell*. We have:

$$V^* = V_{LC} + V_{AC} \tag{5}$$

Where V_{LC} and V_{AC} denote the volume of *Load Cell* and *Adsorption Cell*, respectively. V^V is considered to be equal to the volume occupied by the adsorbent ($V^V = V^S$). Moreover, the density of the gas phase can be determined based on the real gas equation of state:

$$\rho^f = \frac{PM^f}{ZRT} \tag{6}$$

Where, P, T, and R are pressure (kPa), temperature (K), and universal gas constant (kPa.m^3/mol.K), respectively. Z is the compressibility factor of the sorptive gas mixture, which is a function of pressure, temperature, and gas phase composition. M^f (kg/kmol) is the molecular weight of the gas mixture defined as:

$$M^f = \sum_{i=1}^{N} M_i \, y_i \tag{7}$$

Where, y_i is the gas molar composition and M_i (kg/kmol), denotes the molecular weight of each constituent. Eq. (4) can also be written for each component *i* in the gas mixture remaining on the surface of the solid at the equilibrium state:

$$m^f \omega_i^f = \rho^f \omega_i^f (V^* - V^V) \tag{8}$$

Where, ω_i^f is the mass composition of component *i* in the bulk gas phase (not adsorbed), which can be determined experimentally by gas chromatography. Eq. (9) can be expressed in a reduced form as:

$$m_i^f = \rho_i^f (V^* - V^V) \tag{9}$$

By combining Eq. (9) with the overall mass balance for component *i* (Eq. 3), we have:

$$m_i^* = \rho_i^f (V^* - V^V) + m_i \tag{10}$$

Rearranging Eq. (11) to obtain the mass of each component in the adsorbed phase, gives:

$$m_i = \left(m_i^* - \rho_i^f V^*\right) + \rho_i^f V^V \tag{11}$$

$$m_i = \Omega_i + \rho_i^f V^V \tag{12}$$

Where Ω_i is the reduced mass adsorbed of component *i*. As an auxiliary quantity for Ω_i, we have:

$$\Omega_i = m_i^* - \rho_i^f V^* \tag{13}$$

Therefore, m_i can be determined using Eq. (12) and taking Eq. (13). Finally, separation factor of component α (i.e. CO_2) over component β (i.e. H_2) can be calculated using Eq. (14), where *x* and *y* are associated with the molar fractions of each component at the solid and gas phases, respectively. Moreover, superscripts *a* and *f* denote the adsorbed phase (determined by the theoretical concept described above) and remaining phase (not adsorbed) (determined by GC analysis), respectively.

$$S_{\alpha\beta} = \frac{\left(x_\alpha^a / y_\alpha^f\right)}{\left(x_\beta^a / y_\beta^f\right)} \tag{14}$$

3. Results and Discussion

3.1. FT-IR Analysis

In order to explore the presence of functional groups formed on AC surfaces, FT-IR analysis was employed in the range of 400 to 4000 cm^{-1}. Figure 2 represents the FT-IR peaks of as-synthetized AC, prior and after acid treatment with HNO_3 solution. It is worth mentioning that, HNO_3 treatment could result in the presence of various surface functional groups such as carboxyl [29, 30], carbonyl, and nitro groups [31, 32]. While carboxyl groups may play the role of nucleation sites for AC@MOF composite formation [33], carbonyl and nitro groups have the merit of high CO_2 and CH_4 affinity desirable for CO_2/H_2 and CH_4/H_2 separation purposes [27]. According to FT-IR analysis (Fig. 2), bands around 1200-1300, 1700-1800, and 3200-3600 cm^{-1}, which are associated with the presence of (C−O), (C=O), and (O−H) functional groups, respectively, confirm the presence of carboxyl groups on the surface of AC. Besides, strong bands around 1300-1390 cm^{-1} and 1500-1600 cm^{-1} could be attributed to the presence of nitro functional groups (NO_2), i.e. (N−O) symmetric stretch and (N−O) asymmetric stretch, respectively [27, 34]. In addition, the band existed around

1665-1760 cm^{-1} could be translated as presence of carbonyl functional groups as shows in Figure 2.

3.2. XRD Analysis

Figure 3 shows the PXRD patterns of bare *CuBTC* and *AC/CuBTC* composite (i.e. *AC-050/CuBTC* sample). Vividly, there is a good consistency between the position of XRD peaks associated with the *CuBTC* samples and what is reported in the literature [35-37]. All samples possess sharp peaks at around 6.8, 9.6, 11.7, and 13.5 degrees, which can be respectively assigned to (200), (220), (222), and (400) crystal planes of CuBTC. Moreover, the position of peaks associated with the *AC-050/CuBTC* composite does not shift in comparison to *CuBTC* sample. This finding confirms that the crystalline matrix of CuBTC is not affected by AC loading.

In the case of crystal size by the Scherrer equation, as is summarized in Table 2, about the composite sample, although the mean crystal size of *AC-050/CuBTC* composite decreased in comparison to bare *CuBTC*, probably due to the amorphous nature of AC added, the intensity (height) of PXRD peaks increased. We believe that, this observation can be due to the formation of a more ordered CuBTC structure in the presence of carboxyl functionalized AC, which plays the role of nucleation sites.

3.3. Nitrogen Adsorption/Desorption Analysis

Table 3 summarizes the textural properties of the synthesized samples. As observed, the BET surface area and pore volume of the AC-050/CuBTC composite are lower than those of the pristine CuBTC material. Notably, the literature reveals a considerable disparity regarding the influence of various carbon-based additives on the textural characteristics of MOF-based composites. Table 4 qualitatively outlines the effects of combining different carbonaceous materials with metal–organic frameworks on the structural features of the resulting composites. These variations are likely attributed not only to the inherent differences in the original surface and porosity characteristics of the carbonaceous components and inconsistencies in synthesis procedures, but also to the structural diversity of the MOF hosts themselves.

Figures (4a-c) represent nitrogen adsorption/desorption isotherms for *AC*, *bare CuBTC*, and *AC-050/CuBTC* samples, respectively. As could be seen, N_2 adsorption/desorption isotherms for all synthesized samples are following IUPAC type (I) behavior, which suggests the dominance of the micro-porous structure of these porous solids [43]. On the other hand, Figs. 4d to f depict BJH plots (the meso-pore size distribution) and also MP plots (the micro-pore size distribution, Figure insets) associated with *AC*, *bare CuBTC*, and *AC-050/CuBTC* samples, respectively.

BJH/MP plots demonstrate the existence of hierarchical porosities of micro-pores (<2 nm), meso-pores (2–50 nm), and macro-pores (>50 nm) within the matrix of as-synthesized porous solids [44].

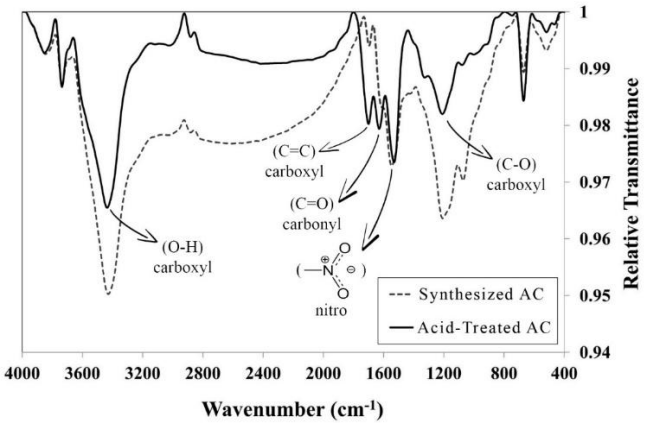

Fig.2. FT-IR spectra of as-synthetized AC prior and after acid treatment with HNO_3

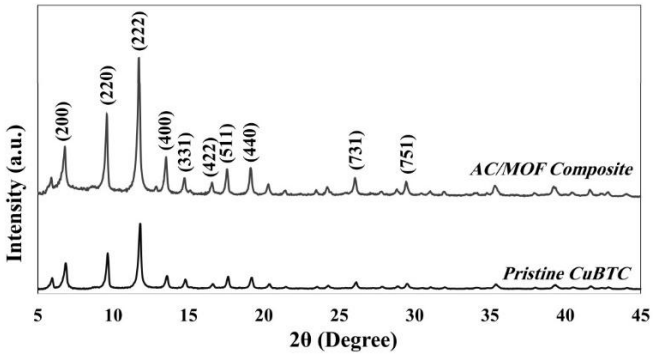

Fig. 3. PXRD patterns of bare CuBTC and AC-050/CuBTC composite

Table 2. Mean crystal size of CuBTC and AC-050/CuBTC composite using Scherrer equation

CuBTC			***AC-050/CuBTC***		
Peak Position (deg, 2θ)	**fwhm (deg)**	**τ (nm)**	**Peak Position (deg, 2θ)**	**fwhm (deg)**	**τ (nm)**
6.788	0.130	60.513	6.779	0.160	49.167
9.581	0.110	71.641	9.565	0.140	56.288
11.714	0.150	52.628	11.720	0.128	61.712
13.506	0.200	39.539	13.489	0.174	45.446
14.727	0.157	50.435	14.716	0.180	43.990
16.548	0.130	61.043	16.540	0.182	43.601
17.553	0.162	49.0450	17.540	0.167	47.580
19.115	0.165	48.264	19.109	0.177	44.991
26.057	0.160	50.378	26.028	0.177	45.537
29.451	0.180	45.109	29.431	0.160	50.745
average crystal size (nm):		**52.860**			**48.906**

τ: crystal size

Table 3. Textural properties of as-synthesized samples.

Sample	**BET (m^2/g)**	**Pore Volume (cm^3/g)**	**Mean Pore Diameter (nm)**
AC	1635	0.9043	2.2118
CuBTC	1689	0.7095	1.6805
AC-050/CuBTC	1630	0.6634	1.6284

Table 4. Impact of Carbon Additives on MOF Textural Properties

Composite	**Surface Area**	**Pore Volume**	**Reference**
AC@MIL-101	increase	decrease	[38]
AC@MIL-101	increase	increase	[17]
AC/MIL-101(Cr)	decrease	---	[20]
AC/MIL 88B (Fe)	increase	decrease	[39]
AC@MIL-101 (Cr)	increase	increase	[40]
CNT@CuBTC	decrease	increase	[7]
CNT@MOF-5	increase	increase	[8]
GrO@CuBTC	increase	increase	[41]
MOF-5@AC	decrease	increase	[42]
CuBDC@AC	decrease	increase	[42]
AC@CuBTC	decrease	decrease	this work

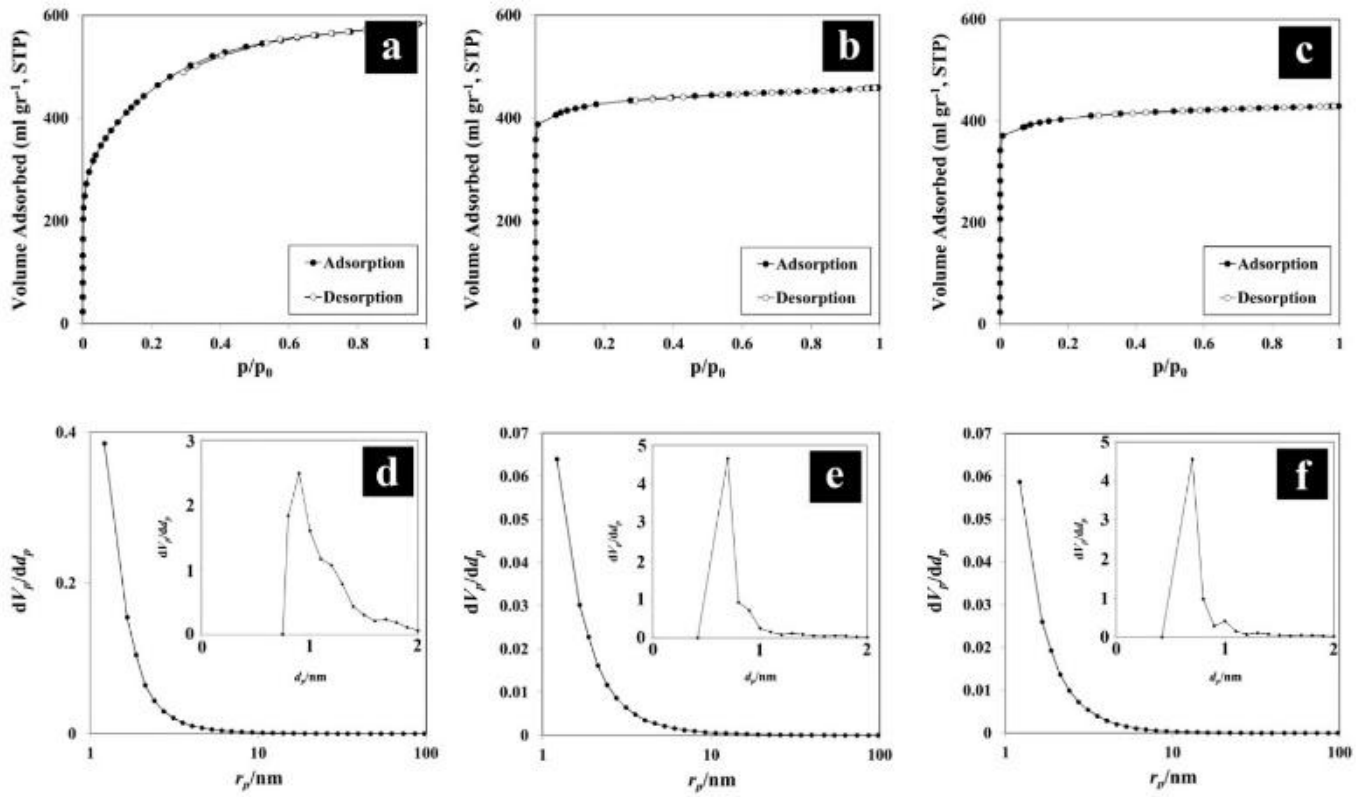

Fig.4. Nitrogen adsorption/desorption isotherms for a) AC, b) bare CuBTC, and c) AC-050/CuBTC samples; BJH/MP (insets) plots of d) AC, e) bare CuBTC, f) AC-050/CuBTC samples.

In addition, according to MP plots (Figs. 4d-f, insets), it is clear that the pore size of all samples is distributed below 2 nm, which confirms the micro-porous structure of all samples mentioned above following IUPAC type (I) isotherms. Besides, by comparing MP plots of *AC-050/CuBTC* with *bare CuBTC* sample (Fig. 4e and f, inset), one can conclude that, *AC-050/CuBTC* contains a local maximum around 1 nm, which might be attributed to the addition of *AC* particles (with micro-porous structure especially around 1 nm, Fig. 4d, inset) into the CuBTC matrix.

Figures 4a to c represent nitrogen adsorption/desorption isotherms for *AC*, *bare CuBTC*, and *AC-050/CuBTC* samples, respectively. As could be seen, N_2 adsorption/desorption isotherms for all synthesized samples are following IUPAC type (I) behavior, which suggests the dominance of the micro-porous structure of these porous solids [43]. On the other hand, Figs. 4d to f depict BJH plots (the meso-pore size distribution) and also MP plots (the micro-pore size distribution, Figure insets) associated with *AC*, *bare CuBTC*, and *AC-050/CuBTC* samples, respectively. BJH/MP plots demonstrate the existence of hierarchical porosities of micro-pores (<2 nm), meso-pores (2–50 nm), and macro-pores (>50 nm) within the matrix of as-synthesized porous solids [44]. In addition, according to MP plots (Figs. 4d-f, insets), it is clear that the pore size of all samples is distributed below 2 nm, which confirms the micro-porous structure of all samples mentioned above following IUPAC type (I) isotherms. Besides, by comparing MP plots of *AC-050/CuBTC* with *bare CuBTC* sample (Fig. 4e and f, inset), one can conclude that, *AC-050/CuBTC* contains a local maximum around 1 nm, which might be attributed to the addition of *AC* particles (with micro-porous structure especially around 1 nm, Fig. 4d, inset) into the CuBTC matrix.

3.4. FESEM Analysis

Detailed morphology and microstructure of AC and AC/MOF samples were examined using FESEM analysis. Figures 5a and 5b illustrate the results for the *AC* and *AC-050/CuBTC* samples, respectively. As can be seen, both *CuBTC* and *AC/CuBTC* samples comprise of octahedral structures similar to CuBTC images reported before [36, 45, 46]. This observation indicates that forming AC/CuBTC composite by integrating activated carbon into the synthesis process does not alter the fundamental structure of the CuBTC framework. Furthermore, the crystal size of the *AC-050/CuBTC* sample appears to be smaller than that typically observed for CuBTC synthesized at temperatures exceeding 100 °C, where an average size of approximately 1 µm is commonly reported [47].

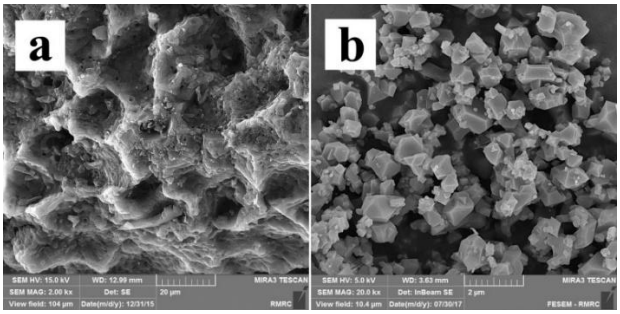

Fig. 5. FESEM images of a) *AC* and b) *AC-050/CuBTC* samples

3.5. Impact of AC Content on CO_2/H_2 Separation

For the separation of gaseous mixtures, there are two main phenomena influencing the separation behavior of a porous solid: the molecular sieving effect and preferential adsorption. Zhao et al. [48] reported that for gas separation purposes, MOF structures possessing pores with a diameter larger than 0.7 nm (such as CuBTC), show the best separation performance based on preferential adsorption. In addition, Yan et al. [49] demonstrated that at low pressures (<1.2 bar) and low temperatures, chemical characteristics of pore surfaces would mainly dictate the adsorptive properties of MOFs.

Figure 6 represents the separation behavior of bare *CuBTC* as well as *AC/CuBTC* composite samples for CO_2/H_2 separation at atmospheric pressure and 273 K, calculated according to the method reported in the previous section. In the case of the *CuBTC* sample, the observed high CO_2/H_2 selectivity (i.e., ≈15) might be owing to the presence of open Cu^{2+} metal sites with high affinity to CO_2 molecules as reported before [50, 51]. However, as one can see, by increasing the amount of AC in the *AC/CuBTC* composite, the CO_2/H_2 separation factor experienced a decreasing-increasing trend. We believe that, this observation might be owing to competitive effects of the presence of open Cu^{2+} metal sites of CuBTC and the grafting functional groups available on the surface of activated carbon to adsorb CO_2 molecules. In other words, while the functional groups on activated carbon have a high tendency to adsorb CO_2 molecules, they also occupy the open Cu^{2+} metal sites, which are known as CO_2 adsorptive nodes of CuBTC, to form the AC/CuBTC composite. This fact may be the reason why CO_2/H_2 selectivity decreased by adding AC up to 0.005 g into the synthesis solution. However, by adding more amounts of AC with nitro and carbonyl groups (i.e., 0.010 and 0.050 g), the effect of excessive functional groups within the composite mixture to adsorb CO_2 would be dominant, and the lack of occupied Cu^{2+} open metal sites would be compensated, which may result in higher CO_2 selectivity over H_2.

4. Conclusions

In this study, AC/CuBTC composites were synthesized via a solvothermal method and evaluated for their CO_2/H_2 separation performance. The findings indicate that the presence of activated carbon (AC) in the composite structure does not notably alter the crystallinity of the CuBTC framework. However, the introduction of 0.050 g of acid-treated AC during synthesis led to a substantial increase in the separation factor, achieving values around 30, approximately twice that of the pristine CuBTC (i.e., ~15), as measured by a volumetric–chromatographic technique. This improved selectivity is likely attributed to the quadrupole nature of CO_2 and the abundance of carbonyl and nitro functional groups present on the AC surface, which enhance CO_2 adsorption within the composite matrix. The outcomes of this research highlight the potential of integrating cost-effective carbonaceous material into MOF-based systems to significantly boost separation efficiency compared to the individual components alone.

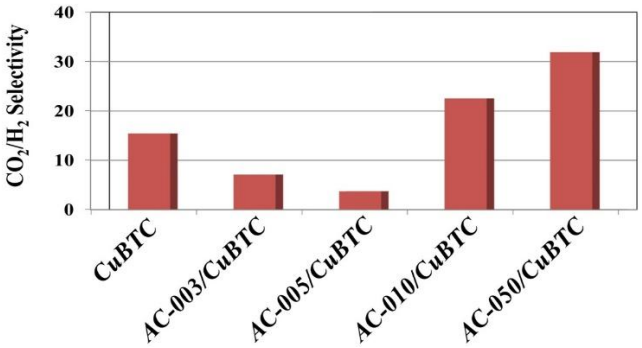

Fig. 6. CO_2/H_2 selectivity of bare *CuBTC* and as-synthesized *AC/CuBTC* composites

References

[1] Q. Yang, C. Zhong, Molecular simulation of carbon dioxide/methane/hydrogen mixture adsorption in metal-organic frameworks, J. Phys. Chem. B. 110(36) (2006) 17776-17783, https://doi.org/10.1021/jp062723w.

[2] S. Sircar, T. Golden, Purification of hydrogen by pressure swing adsorption, Sep. Sci. Technol. 35(5) (2000) 667-687, https://doi.org/10.1081/SS-100100183

[3] J. Hufton, S. Mayorga, S. Sircar, Sorption-enhanced reaction process for hydrogen production, AIChE J. 45(2) (1999) 248-256, https://doi.org/10.1002/aic.690450205.

[4] R.J. Kuppler, D.J. Timmons, Q.-R. Fang, J.-R. Li, T.A. Makal, M.D. Young, D. Yuan, D. Zhao, W. Zhuang, H.-C. Zhou, Potential applications of metal-organic frameworks, Coord. Chem. Rev. 253(23-24) (2009) 3042-3066, https://doi.org/10.1016/j.ccr.2009.05.019.

[5] D. Zhao, D. Yuan, D. Sun, H.-C. Zhou, Stabilization of metal− organic frameworks with high surface areas by the incorporation of mesocavities with microwindows, J. Am. Chem. Soc. 131(26) (2009) 9186-9188, https://doi.org/10.1021/ja901109t.

[6] Z. Xiang, X. Peng, X. Cheng, X. Li, D. Cao, CNT@Cu3(BTC)2 and metal–organic frameworks for separation of CO2/CH4 mixture, J. Phys. Chem. C. 115(40) (2011) 19864-19871, https://doi.org/10.1021/jp206959k.

[7] Z. Xiang, Z. Hu, D. Cao, W. Yang, J. Lu, B. Han, W. Wang, Metal–organic frameworks with incorporated carbon nanotubes: improving carbon dioxide and methane storage capacities by lithium doping, Angew. Chem. Int. Ed. 50(2) (2011) 491-494, https://doi.org/10.1002/anie.201004537.

[8] S.J. Yang, J.Y. Choi, H.K. Chae, J.H. Cho, K.S. Nahm, C.R. Park, Preparation and enhanced hydrostability and hydrogen storage capacity of CNT@MOF-5 hybrid composite, Chem. Mat. 21(9) (2009) 1893-1897, https://doi.org/10.1021/cm803502y.

[9] K. Prasanth, P. Rallapalli, M.C. Raj, H. Bajaj, R.V. Jasra, Enhanced hydrogen sorption in single walled carbon nanotube incorporated MIL-101 composite metal-organic framework, Int. J. Hydrogen Energy. 36(13) (2011) 7594-7601, https://doi.org/10.1016/j.ijhydene.2011.03.109.

[10] S. Sun, Y. Wang, L. Chen, M. Chu, Y. Dong, D. Liu, P. Liu, D. Qu, J. Duan, X. Li, MOF (Ni)/CNT composites with layer structure for high capacitive performance, Colloids Surf. A Physicochem. Eng. Asp. 643 (2022) 128802, https://doi.org/10.1016/j.colsurfa.2022.128802.

[11] H. Huang, Y. Chen, Z. Chen, J. Chen, Y. Hu, J.-J. Zhu, Electrochemical sensor based on Ce-MOF/carbon nanotube composite for the simultaneous discrimination of hydroquinone and catechol, J. Hazard. Mater. 416 (2021) 125895, https://doi.org/10.1016/j.jhazmat.2021.125895.

[12] A. Huang, Y. Chen, Q. Liu, N. Wang, J. Jiang, J. Caro, Synthesis of highly hydrophobic and permselective metal–organic framework Zn (BDC)(TED) 0.5 membranes for H2/CO2 separation, J. Membr. Sci. 454 (2014) 126-132, https://doi.org/10.1016/j.memsci.2013.12.018.

[13] T.J. Bandosz, C. Petit, MOF/graphite oxide hybrid materials: exploring the new concept of adsorbents and catalysts, Adsorption 17(1) (2011) 5-16, https://doi.org/10.1007/s10450-010-9267-5.

[14] Y. Zhao, M. Seredych, Q. Zhong, T.J. Bandosz, Aminated graphite oxides and their composites with copper-based metal–organic

framework: in search for efficient media for CO2 sequestration, RSC Adv. 3(25) (2013) 9932-9941, https://doi.org/10.1039/C3RA40817E.
[15] S. Gautam, S. Rialach, S. Paul, N. Goyal, MOF/graphene oxide based composites in smart supercapacitors: a comprehensive review on the electrochemical evaluation and material development for advanced energy storage devices, RSC Adv. 14(20) (2024) 14311-14339, https://doi.org/10.1039/D4RA01027B.
[16] H.C. Bajaj, R.S. Somani, P.B. Rallapalli, D. Patil, K.P. Prasanth, C.R. Manoj, R.S. Thakur, M. John, B.L. Newalkar, N.V. Choudary, Activated carbon-metal organic framework composite materials with enhanced gas adsorption capacity and process for the preparation thereof, Google Patents, 2014.
[17] P. Somayajulu Rallapalli, M.C. Raj, D.V. Patil, K. Prasanth, R.S. Somani, H.C. Bajaj, Activated carbon@MIL-101(Cr): a potential metal-organic framework composite material for hydrogen storage, Int. J. Energy Res. 37(7) (2013) 746-753, https://doi.org/10.1002/er.1933.
[18] S.-Y. Lee, S.-J. Park, Effect of platinum doping of activated carbon on hydrogen storage behaviors of metal-organic frameworks-5, Int. J. Hydrogen Energy. 36(14) (2011) 8381-8387, https://doi.org/10.1016/j.ijhydene.2011.03.038.
[19] P.K. Prabhakaran, J. Deschamps, Doping activated carbon incorporated composite MIL-101 using lithium: impact on hydrogen uptake, J. Mater. Chem. A 3(13) (2015) 7014-7021, https://doi.org/10.1039/C4TA07197B.
[20] N.M. Mahmoodi, M. Taghizadeh, A. Taghizadeh, Activated carbon/metal-organic framework composite as a bio-based novel green adsorbent: Preparation and mathematical pollutant removal modeling, J. Mol. Liq. 277 (2019) 310-322, https://doi.org/10.1016/j.molliq.2018.12.050.
[21] L.N. McHugh, A. Terracina, P.S. Wheatley, G. Buscarino, M.W. Smith, R.E. Morris, Metal–Organic Framework-Activated Carbon Composite Materials for the Removal of Ammonia from Contaminated Airstreams, Angew. Chem. Int. Ed. 58(34) (2019) 11747-11751, https://doi.org/10.1002/ange.201905779.
[22] K. Esfandiari, A.R. Mahdavi, A.A. Ghoreyshi, M. Jahanshahi, Optimizing parameters affecting synthetize of CuBTC using response surface methodology and development of AC@ CuBTC composite for enhanced hydrogen uptake, Int. J. Hydrogen Energy. 43(13) (2018) 6654-6665, https://doi.org/10.1016/j.ijhydene.2018.02.089.
[23] Y.-C. Chiang, C.-Y. Yeh, C.-H. Weng, Carbon dioxide adsorption on porous and functionalized activated carbon fibers, Appl. Sci. 9(10) (2019) 1977, https://doi.org/10.3390/app9101977.
[24] D. Vargas, L. Giraldo, A. Erto, J. Moreno-Piraján, Chemical modification of activated carbon monoliths for CO2 adsorption, J. Therm. Anal. Calorim. 114(3) (2013) 1039-1047, https://doi.org/10.1007/s10973-013-3086-3.
[25] B.S. Caglayan, A.E. Aksoylu, CO2 adsorption on chemically modified activated carbon, J. Hazard. Mater. 252 (2013) 19-28, https://doi.org/10.1016/j.jhazmat.2013.02.028.
[26] E. Mehrvarz, A.A. Ghoreyshi, M. Jahanshahi, Surface modification of broom sorghum-based activated carbon via functionalization with triethylenetetramine and urea for CO2 capture enhancement, Front. chem. eng. 11(2) (2017) 252-265, https://doi.org/10.1007/s11705-017-1630-6.
[27] M.S. Shafeeyan, W.M.A.W. Daud, A. Houshmand, A. Shamiri, A review on surface modification of activated carbon for carbon dioxide adsorption, J. Anal. Appl. Pyrolysis. 89(2) (2010) 143-151, https://doi.org/10.1016/j.jaap.2010.07.006.
[28] J.U. Keller, R. Staudt, Volumetric-Gravimetric Measurements, Gas Adsorption Equilibria, Experimental Methods and Adsorptive Isotherms, Springer, 2005, pp. 181-235.
[29] W. Shen, Z. Li, Y. Liu, Surface chemical functional groups modification of porous carbon, Recent Patents on Chemical Engineering 1(1) (2008) 27-40.
[30] Z. Tang, Y. Zhang, M.M. Maroto-Valer, Study of the CO2 adsorption capacities of modified activated anthracites, Prepr. Pap.-Am. Chem. Soc., Div. Fuel Chem 49(1) (2004) 308-309.
[31] J.P. Chen, S. Wu, Acid/base-treated activated carbons: characterization of functional groups and metal adsorptive properties, Langmuir 20(6) (2004) 2233-2242, https://doi.org/10.1021/la0348463.
[32] V. Gomez-Serrano, M. Acedo-Ramos, A. Lopez-Peinado, C. Valenzuela-Calahorro, Mass and surface changes of activated carbon treated with nitric acid. Thermal behavior of the samples,
Thermochim. Acta 291(1-2) (1997) 109-115, https://doi.org/10.1016/S0040-6031(96)03098-5.
[33] M. Shoaee, M.W. Anderson, M.P. Attfield, Crystal Growth of the Nanoporous Metal-Organic Framework HKUST-1 Revealed by In Situ Atomic Force Microscopy, Angew. Chem. 120(44) (2008) 8653-8656, https://doi.org/10.1002/anie.200803460.
[34] I.I. Salame, T.J. Bandosz, Surface chemistry of activated carbons: combining the results of temperature-programmed desorption, Boehm, and potentiometric titrations, J. Colloid Interface Sci. 240(1) (2001) 252-258, https://doi.org/10.1006/jcis.2001.7596.
[35] M. Hartmann, S. Kunz, D. Himsl, O. Tangermann, S. Ernst, A. Wagener, Adsorptive separation of isobutene and isobutane on Cu3(BTC)2, Langmuir 24(16) (2008) 8634-8642, https://doi.org/10.1021/la8008656.
[36] K. Pirzadeh, A.A. Ghoreyshi, M. Rahimnejad, M. Mohammadi, Electrochemical synthesis, characterization and application of a microstructure Cu3(BTC)2 metal organic framework for CO2 and CH4 separation, Korean j. chem. eng. (2018) 1-10, https://doi.org/10.1007/s11814-017-0340-6.
[37] S. Khoshhal, A.A. Ghoreyshi, M. Jahanshahi, M. Mohammadi, Study of the temperature and solvent content effects on the structure of Cu–BTC metal organic framework for hydrogen storage, RSC Adv. 5(31) (2015) 24758-24768, https://doi.org/10.1039/C5RA01890K.
[38] P.K. Prabhakaran, L. Catoire, J. Deschamps, Aluminium doping composite metal-organic framework by alane nanoconfinement: Impact on the room temperature hydrogen uptake, Microporous Mesoporous Mater. 243 (2017) 214-220, https://doi.org/10.1016/j.micromeso.2017.02.032.
[39] N.M. Mahmoodi, J. Abdi, M. Taghizadeh, A. Taghizadeh, B. Hayati, A.A. Shekarchi, M. Vossoughi, Activated carbon/metal-organic framework nanocomposite: Preparation and photocatalytic dye degradation mathematical modeling from wastewater by least squares support vector machine, J. Environ. Manag. 233 (2019) 660-672, https://doi.org/10.1016/j.jenvman.2018.12.026.
[40] M. Hasanzadeh, A. Simchi, H.S. Far, Nanoporous composites of activated carbon-metal organic frameworks for organic dye adsorption: Synthesis, adsorption mechanism and kinetics studies, J. Ind. Eng. Chem. 81 (2020) 405-414, https://doi.org/10.1016/j.jiec.2019.09.031.
[41] W. Huang, X. Zhou, Q. Xia, J. Peng, H. Wang, Z. Li, Preparation and adsorption performance of GrO@Cu-BTC for separation of CO2/CH4, Ind. Eng. Chem. Res. 53(27) (2014) 11176-11184, https://doi.org/10.1021/ie501040s.
[42] N.Y. Nikravesh, M. Beygzadeh, M. Adl, Microporous MOF-5@ AC and Cu-BDC@AC Composite Materials for Methane Storage in ANG Technology, Int. J. Energy Res. 2023(1) (2023) 2282746, https://doi.org/10.1155/2023/2282746.
[43] K.S. Sing, Reporting physisorption data for gas/solid systems with special reference to the determination of surface area and porosity (Recommendations 1984), Pure Appl. Chem. 57(4) (1985) 603-619, https://doi.org/10.1351/pac198254112201.
[44] D.W. Wang, F. Li, M. Liu, G.Q. Lu, H.M. Cheng, 3D aperiodic hierarchical porous graphitic carbon material for high-rate electrochemical capacitive energy storage, Angew. Chem. Int. Ed. 47(2) (2008) 373-376, https://doi.org/10.1002/anie.200702721.
[45] K.-S. Lin, A.K. Adhikari, C.-N. Ku, C.-L. Chiang, H. Kuo, Synthesis and characterization of porous HKUST-1 metal organic frameworks for hydrogen storage, Int. J. Hydrogen Energy. 37(18) (2012) 13865-13871, https://doi.org/10.1016/j.ijhydene.2012.04.105.
[46] J. Kim, H.-Y. Cho, W.-S. Ahn, Synthesis and adsorption/catalytic properties of the metal organic framework CuBTC, Catal. Surv. Asia. 16(2) (2012) 106-119, https://doi.org/10.1007/s10563-012-9135-2.
[47] K. Schlichte, T. Kratzke, S. Kaskel, Improved synthesis, thermal stability and catalytic properties of the metal-organic framework compound Cu3(BTC)2, Microporous Mesoporous Mater. 73(1-2) (2004) 81-88, https://doi.org/10.1016/j.micromeso.2003.12.027.
[48] Z. Zhao, X. Ma, A. Kasik, Z. Li, Y. Lin, Gas separation properties of metal organic framework (MOF-5) membranes, Ind. amp; Eng. Chem. Res. 52(3) (2012) 1102-1108, https://doi.org/10.1021/ie202777q.
[49] X. Yan, S. Komarneni, Z. Zhang, Z. Yan, Extremely enhanced CO2 uptake by HKUST-1 metal–organic framework via a simple chemical treatment, Microporous Mesoporous Mater. 183 (2014) 69-73, https://doi.org/10.1016/j.micromeso.2013.09.009.
[50] Y. Liu, Z.U. Wang, H.C. Zhou, Recent advances in carbon dioxide capture with metal-organic frameworks, Greenhouse Gases: Sci. Technol. 2(4) (2012) 239-259, https://doi.org/10.1002/ghg.1296.
[51] K. Esfandiari, A.A. Ghoreyshi, M. Jahanshahi, Using Artificial Neural Network and Ideal Adsorbed Solution Theory for Predicting the CO2/CH4 Selectivities of Metal–Organic Frameworks: A Comparative Study, Ind. Eng. Chem. Res. 56(49) (2017) 14610-14622, https://doi.org/10.1021/acs.iecr.7b03008.